Forecast, measurement, and modeling of an unprecedented polar ozone filament event over Mauna Loa Observatory, Hawaii

Om Prakash Tripathi, Thierry Leblanc, I. Stuart Mcdermid, Frank Lefèvre, Marion Marchand, Alain Hauchecorne

Forecast, measurement, and modeling of an unprecedented polar ozone filament event over Mauna Loa Observatory, Hawaii

Om Prakash Tripathi,[1] Thierry Leblanc,[1] I. Stuart McDermid,[1] Frank Lefèvre,[2] Marion Marchand,[2] and Alain Hauchecorne[2]

Received 8 February 2006; revised 26 May 2006; accepted 26 June 2006; published 21 October 2006.

[1] In mid-March 2005 the northern lower stratospheric polar vortex experienced a severe stretching episode, bringing a large polar filament far south of Alaska toward Hawaii. This meridional intrusion of rare extent, coinciding with the polar vortex final warming and breakdown, was followed by a zonal stretching in the wake of the easterly propagating subtropical main flow. This caused polar air to remain over Hawaii for several days before diluting into the subtropics. After being successfully forecasted to pass over Hawaii by the high-resolution potential vorticity advection model Modèle Isentrope du transport Méso-échelle de l'Ozone Stratosphérique par Advection (MIMOSA), the filament was observed on isentropic surfaces between 415 K and 455 K (17–20 km) by the Jet Propulsion Laboratory stratospheric ozone lidar measurements at Mauna Loa Observatory, Hawaii, between 16 and 19 March 2005. It was materialized as a thin layer of enhanced ozone peaking at 1.6 ppmv in a region where the climatological values usually average 1.0 ppmv. These values were compared to those obtained by the three-dimensional Chemistry-Transport Model MIMOSA-CHIM. Agreement between lidar and model was excellent, particularly in the similar appearance of the ozone peak near 435 K (18.5 km) on 16 March, and the persistence of this layer at higher isentropic levels for the following three days. Passive ozone, also modeled by MIMOSA-CHIM, was at about 3–4 ppmv inside the filament while above Hawaii. A detailed history of the modeled chemistry inside the filament suggests that the air mass was still polar ozone–depleted when passing over Hawaii. The filament quickly separated from the main vortex after its Hawaiian overpass. It never reconnected and, in less than 10 days, dispersed entirely in the subtropics.

Citation: Tripathi, O. P., T. Leblanc, I. S. McDermid, F. Lefèvre, M. Marchand, and A. Hauchecorne (2006), Forecast, measurement, and modeling of an unprecedented polar ozone filament event over Mauna Loa Observatory, Hawaii, *J. Geophys. Res.*, *111*, D20308, doi:10.1029/2006JD007177.

1. Introduction

[2] Rossby waves are one of the dominant sources of variability in the lower stratosphere, in particular during the Northern Hemisphere winter and spring. Wave-breaking events transport air masses from the polar vortex to the middle and lower latitudes in the form of long filamentary structures [*Waugh et al.*, 1994], and mix with surrounding midlatitude air throughout the winter and spring season [*Plumb et al.*, 1994]. This type of event is also considered one of the causes of midlatitude ozone decrease [*Stolarski et al.*, 1992; *Knudsen and Grooß*, 2000] through the transfer of chemically perturbed air ejected out of the polar vortex to the midlatitudes [*Tuck et al.*, 1992]. Using a photochemical trajectory model, *Reid et al.* [1998] have shown that the air in ozone filaments advected across Europe in February 1995 was chemically activated and had an impact on the midlatitude ozone concentration. If the air parcels contain a high level of chlorine monoxide they trigger in situ chemical ozone destruction in the midlatitudes [*World Meteorological Organization* (*WMO*), 1998].

[3] The study of filamentation and air transport from the polar vortex to middle and lower latitudes is therefore of great importance to better understand recently observed ozone trends in midlatitudes. Many recent studies [*Dahlberg and Bowman*, 1994; *Waugh et al.*, 1994; *Hauchecorne et al.*, 2002; *Godin et al.*, 2002; *Marchand et al.*, 2003] have documented the quantitative and qualitative impact of filaments on the midlatitude ozone reservoir. In general the scales involved in these events are synoptic or subsynoptic, and high-resolution simulations are needed for detailed investigation of the phenomenon. Various methods such as reverse domain-filling trajectories [*Orsolini et al.*, 1997], contour advection with surgery [*Waugh et al.*, 1994; *Mariotti et al.*, 1997], and potential vorticity (PV) advection

[1] Table Mountain Facility, Jet Propulsion Laboratory, California Institute of Technology, Wrightwood, California, USA.
[2] Service d'Aeronomie du Centre National de la Recherche Scientifique, Université Pierre et Marie Curie, Paris, France.

0148-0227/06/2006JD007177

[*Hauchecorne et al.*, 2002] have been used in the past to study filaments extending to midlatitudes. For example, *Norton and Chipperfield* [1995] used a three-dimensional chemical transport model and a contour advection technique to obtain a high-resolution view of the transport of PSC-activated air. They indicated that there is high interannual variability in the amount of active air transported from the vortex to midlatitude regions.

[4] All the studies cited above mainly concentrated on midlatitude regions because filaments, in general, dilute and mix with surrounding air by the time they reach this region. However, the present paper presents a detailed study of a very exceptional filament that peeled off the polar vortex and stretched far into the tropics. It was detected by the ozone lidar of the Jet Propulsion Laboratory (JPL) located at the Mauna Loa Observatory (MLO), Hawaii (19.5°N, 155.6°W). A few days before it occurred, the ozone-rich filament was forecasted to pass over the lidar station by the Modèle Isentrope du transport Méso-échelle de l'Ozone Stratosphérique par Advection (MIMOSA) [*Hauchecorne et al.*, 2002]. Thanks to this forecast, the filament was successfully probed by the ozone lidar. Ozone modeled by the three-dimensional Chemistry-Transport Model version of MIMOSA (MIMOSA-CHIM) was then compared to that observed by lidar. In section 2 a brief overview of the diagnostic tools used is presented (i.e., the JPL lidar data and the different versions of MIMOSA used). In section 3 the filament case study is presented. It includes forecasting, analysis, and lidar measurements of the event. With the help of 15-day isentropic trajectories, we discuss in sections 4 and 5 the chemical aspects of the event reproduced by MIMOSA-CHIM.

2. Data Sets, Prognostics, and Diagnostic Tools

2.1. JPL Lidar Instrument

[5] In the framework of the Network for the Detection of Atmospheric Composition Change (NDACC, formerly Network for the Detection of Stratospheric Change, NDSC), a Differential Absorption Lidar (DIAL) was deployed at MLO by the JPL lidar group in the early 1990s to provide long-term measurements of stratospheric ozone at near-tropical latitudes [*McDermid et al.*, 1990, 1995]. The system has operated routinely since 1993. The lidar utilizes two excimer lasers in an oscillator-amplifier (MOPA) configuration emitting at 308 nm (the "absorbed" wavelength), and a Nd:YAG laser emitting at 355 nm (the "nonabsorbed" wavelength). After various signal corrections, ozone is retrieved using the DIAL technique, that is, using the "absorption differential" between the signals returned at the two wavelengths. The instrumental sampling interval is 300-m, allowing ozone profiles to be derived with high vertical resolution (~1.2 km) in the lower stratosphere where signal filtering is minimal. The system is operated year-round, four to five nights per week during the first two hours of the night. The results are archived at the worldwide NDACC database (http://www.ndsc.ws). The 10+ year ozone data set obtained from this lidar was used to perform an ozone climatology [*Leblanc and McDermid*, 2000], an early study of the Quasi-Biennial Oscillation (QBO) [*Leblanc and McDermid*, 2001], and a case study of Rossby wave breaking just above the tropopause [*Leblanc et al.*, 2004]. It is also used to validate many instruments onboard various satellite platforms including UARS, ENVISAT, and the latest EOS-Aura. The Microwave Limb Sounder (MLS) onboard EOS-Aura detected the filament presented here, and a comparison of its measurement with the MLO lidar measurement is presented elsewhere [*Leblanc et al.*, 2006].

2.2. High-Resolution Isentropic PV Advection Model MIMOSA

[6] MIMOSA was originally developed at Service d'Aéronomie du CNRS for the European project METRO (Meridional Transport of Ozone in the Lower Stratosphere) to capture and quantify the filamentary structures passing over Europe in winter and spring, and to assess the importance of such structures in the irreversible transport of polar air into midlatitudes [*Hauchecorne et al.*, 2002]. In an idealized adiabatic, frictionless atmosphere, isentropic PV is a conserved tracer with a zonally mean positive latitudinal gradient throughout the stratosphere (i.e., increasing poleward in the Northern Hemisphere), and with a sharper gradient in the regions separating the winter polar vortex from the lower latitudes. Therefore it has tracer characteristics similar to those of ozone in the lower stratosphere and, under conditions of natural ozone balance, we can expect a high degree of correlation between lower stratospheric PV and ozone.

[7] Global analyzed or forecasted isentropic winds and PV (typically coming from the European Centre for Medium-Range Weather Forecasts, ECMWF, or from the National Centers for Environmental Prediction, NCEP) are input to MIMOSA where they are interpolated onto an azimuthal equidistant projection grid with a very fine resolution, typically several points per degree. The PV is advected isentropically using a 1-hour elementary time step and re-interpolated onto a regular longitude-latitude grid. In the present study, the output longitude-latitude grid has been kept identical to the advection model grid, that is, 3 points per degree in latitude and longitude. A careful validation of the chosen interpolation and regridding scheme showed numerical diffusion of the same order as that estimated for the real atmosphere [*Hauchecorne et al.*, 2002]. To account for diabatic processes, the high-resolution PV is relaxed with a 10-day relaxation constant toward the PV extracted from the original model grid (ECMWF or NCEP), and interpolated onto MIMOSA grid. This relaxation technique allows the model to run over several weeks or months with, for example, the diabatic descent inside the winter polar vortex implicitly reproduced. The technique used in MIMOSA (smoothed difference between PV from meteorological analysis and advected PV) assumes that diabatic processes are slow and homogenous on a scale of a few 100 km. Unlike global analysis such as ECMWF or NCEP interpolated onto a very fine grid, the high-resolution PV advection model is able to reproduce the evolution of fine PV structures such as stretching polar filaments without disconnecting them from the main vortex. To illustrate this, the ECMWF T106-analyzed PV fields and high-resolution MIMOSA-advected PV fields at 435 K are shown for 16 March 2005 at 0000 UT in Figure 1 (top and bottom, respectively). On these two maps, the vortex edge is contoured with three white lines (two thin lines being the outer and inner edges, and one thick line being the center

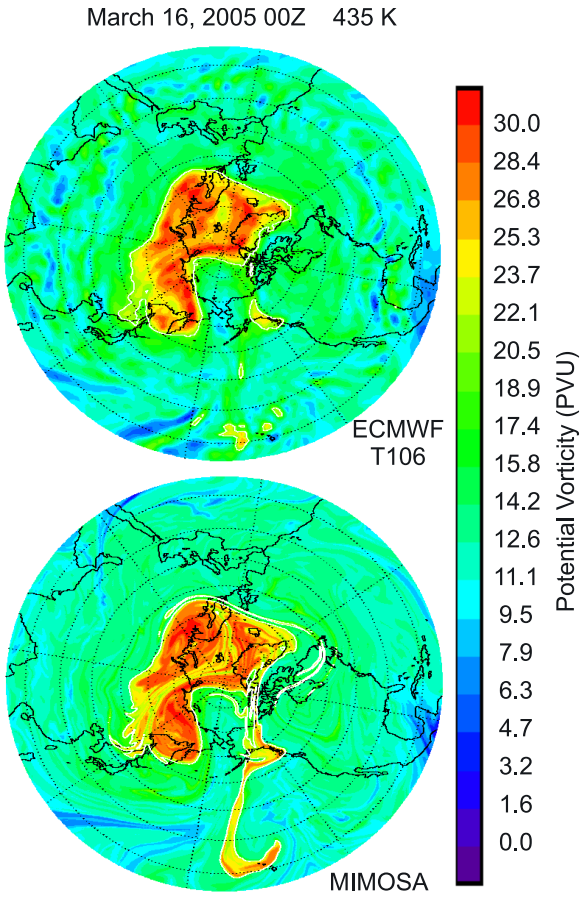

Figure 1. Isentropic potential vorticity (PV) fields at 435 K on 16 March 2005 at 0000 UT, (a) computed from the T106 European Centre for Medium-Range Weather Forecasts (ECMWF) analysis grid and (b) advected using Modèle Isentrope du transport Méso-échelle de l'Ozone Stratosphérique par Advection (MIMOSA).

edge). The large polar filament studied in this paper is largely developed on the MIMOSA advected-PV map, stretching without discontinuity from Alaska to Hawaii. On the other hand, it is barely identifiable on the ECMWF T106 PV map and only a few regions of higher PV can be observed in the vicinity of Hawaii. Note, however, that the improved resolution (T511) of the most recent ECMWF model now allows a better identification of such filaments.

[8] A particularity of a model like MIMOSA is that global winds from various sources can be fed into the model to advect PV. In the present study, the global fields from two state-of-the art models were used. The NCEP operational forecast products from the Global Forecast System (GFS) are used to run MIMOSA in two PV "forecast" modes (see details below), and the isentropic wind fields from the T106 truncated operational ECMWF analysis are used to run MIMOSA in an PV "analysis" mode.

2.2.1. Forecast-Mode Version of MIMOSA at JPL

[9] For the purpose of long-term forecasting (high-resolution PV forecasts up to 168 hours at intervals of 12 hours), the global fields 1.25° × 1.25° from the NCEP GFS model are used. Short-term forecasts (up to 18 hours with 3 hours intervals) are also produced using the forecast products from the NCEP GFS model. The pressure-gridded global fields (1000 hPa to 10 hPa) are interpolated onto 42 isentropic levels from 300 K to 750 K before being fed into the high-resolution PV advection model. The choice of the GFS model was mainly driven by the need for, and easy access to, publicly available data on a near-real-time basis, which has been the case since 1999 at the National Oceanic and Atmospheric Administration (NOAA) ftp site: ftp://ftpprd.ncep.noaa.gov.

2.2.2. Analysis-Mode Version of MIMOSA at JPL

[10] When the use of forecast products is not necessary, the standard version of MIMOSA running at JPL uses the truncated T106 ECMWF global operational analysis (1.125° × 1.125° resolution), available to NDACC participants at the Norwegian Institute for Air Research (NILU), Norway. The model outputs at 6-hour intervals are interpolated onto 55 isentropic levels from 300 K to 2000 K before being fed to the high-resolution PV advection model. ECMWF has undergone major modifications in 1999 [e.g., *Rabier et al.*, 2000]. To study Rossby wave-breaking events near the tropopause, and the long-term evolution of (high-resolution) equivalent latitude at MLO and TMF, MIMOSA has been running nonstop at JPL in this mode since 1999, and has since been producing 4 times daily global high-resolution isentropic PV fields in near-real time (data set updated every 10 days).

2.3. MIMOSA With Chemistry: MIMOSA-CHIM

[11] MIMOSA-CHIM, combines the PV advection scheme described in the previous paragraph (hereinafter referred to as "PV-only"), and the chemistry scheme of the three-dimensional Chemical Transport Model (CTM) REPROBUS (Reactive Processes Ruling the Ozone Budget in the Stratosphere) [*Lefèvre et al.*, 1994; *Marchand et al.*, 2003]. The chemical fields of MIMOSA-CHIM are initialized by the REPROBUS output fields interpolated on isentropic levels and are advected along with PV with a time step of one hour. For several months-long simulations, the diabatic transport of air across isentropic surfaces, and the diabatic evolution of PV have to be taken into account. Diabatic mass fluxes are computed from the heating rates calculated using the radiation scheme of the SLIMCAT model taken from MIDRAD [*Chipperfield*, 1999; *Shine*, 1987]. Climatological water vapor, CO_2, and interactive ozone fields (taken from the model itself) are used for the calculation of heating rates.

[12] For computational reasons, MIMOSA-CHIM could not be run at JPL with the same high-resolution as the PV-only version. Instead, the horizontal resolution is 1° in latitude and longitude. Twenty one vertical levels were used (from 350 K and 950 K with best resolution of 5 K at levels near 430 K, yielding a vertical resolution of about 2 km). Also unlike the PV-only version, the model domain in the chemistry version extends to 10 degrees of latitude in the other hemisphere; that is, the latitude range of the simulation is 10°S–90°N. To take into account the influence of air masses originating from regions outside of the model domain, PV fields of ECMWF and chemical fields of REPROBUS are used for the forcing at the boundary of the model. The complete REPROBUS fields are generally available once a month, so they are interpolated in time for

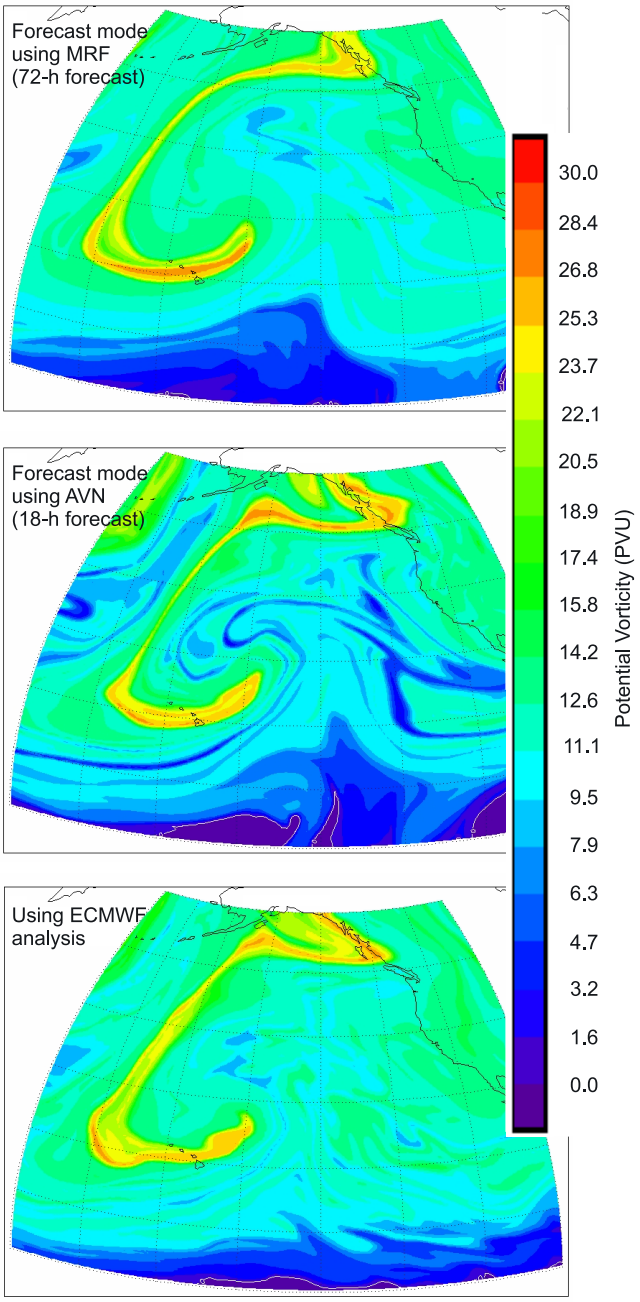

Figure 2. MIMOSA PV fields output at 435 K on 16 March 2005 at 0600 UT, computed using the meteorological fields of the (top) 72-hour Global Forecast System (GFS) forecasts, (middle) 18-hour GFS forecasts, and (bottom) the ECMWF analysis. See text for details.

the forcing at the boundary. Various sensitivity tests have been performed to evaluate the effect of the other hemispheric air masses on the ozone loss in the polar vortex by using forcing fields from different sources. These tests have shown that the effect of forcing fields on the ozone loss inside the vortex remains small, either using REPROBUS data or even climatological fields.

[13] The REPROBUS chemical scheme includes 55 chemical species and about 160 gas phase, heterogeneous, and photolytic reactions [*Lefèvre et al.*, 1994, 1998]. The updated photochemical data of JPL-2002 [*Sander et al.*, 2003] recommendations are implemented for this study. The model has a detailed scheme of liquid and solid PSC formation and growth. The saturation vapor pressure given by *Hanson and Mauersberger* [1988] is used to predict the existence of NAT particles and *Murray* [1967] for water-ice particles. A denitrification scheme is introduced to account for the sedimentation of HNO_3 containing particles where the NAT particles are assumed to be in equilibrium with gas-phase nitric acid. The sedimentation speed of particles is calculated according to *Pruppacher and Klett* [1997]. A constant number density (5.0×10^{-3} cm^{-3}) of NAT particles is considered for the analysis [*Waibel et al.*, 1999]. More detailed description of the model is given by *Tripathi et al.* [2006].

3. The 16 March 2005 Polar Filament Event Over Hawaii: Case Study

3.1. Overview of the Dynamical Context

[14] Around 13 March 2005, the PV-only forecast version of MIMOSA running in real time at JPL triggered a so-called "polar filament alert" at Mauna Loa Observatory (MLO), Hawaii. Such an alert is triggered each time an air mass with characteristics of the polar vortex is forecasted to pass over Table Mountain Facility (California), or Mauna Loa, the locations of the two JPL lidars. Though alerts are not uncommon for Table Mountain, they are extremely rare for Mauna Loa, because of the nearly tropical location of the Hawaiian site. This alert, initially triggered from the 72-hour forecast, was confirmed on every day's forecast until the event actually occurred, on 16–19 March 2005. The southward stretching of the filament coincided in time with the onset of the so-called Northern Hemisphere spring "final warming." Interestingly the pathway used here is very similar to that described by *Orsolini and Grant* [2000] along the eastern and southern edge of the Aleutian Highs.

[15] Figure 2 shows MIMOSA-advected PV maps over the Northeastern Pacific Region on 16 March at 0600 UT and 425 K (18 km), output from the 72-hour forecast (Figure 2, top), the 18-hour forecast (Figure 2, middle), and the ECMWF T106 analysis (Figure 2, bottom). The consistency in the position and timing of the filament is remarkable between both forecasts, and between the forecasts and the analysis. The filament passed over the Big Island of Hawaii (the triangle-shaped southeastern most island of the archipelago) on two occasions: the first time on 16 March, during the main vortex stretching event (as shown on Figure 2), when the filament tip slipped down from Alaska toward Hawaii (main motion was southward), and the second time on 19 March (not shown), when the "elbow" of the filament (i.e., its southwestern edge, located west of the islands on Figure 2) remained stationary for a few hours over the island, just before it initiated a high speed eastward motion toward Southern California. The quality of the forecast allowed the JPL personnel to anticipate optimal ozone lidar measurements on the night of 16 March, and on the following three nights. Only results from 16 March will be described in detail here as little additional information can be drawn from the other nights.

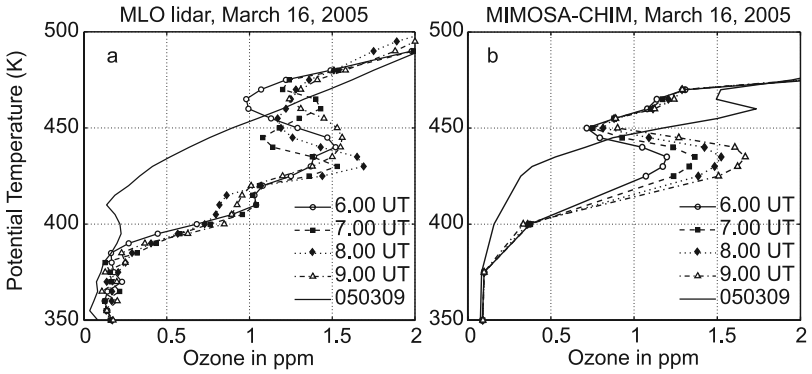

Figure 3. (a) One-hour integrated ozone profiles measured from 0600 to 0900 UT by the Mauna Loa Observatory (MLO) lidar on the night of 16 March 2005. To compare with a typical subtropical latitudes profile, the 2-hour integrated profile of 9 March is also shown. (b) MIMOSA-CHIM ozone profiles modeled at the same times and location as that measured by lidar.

3.2. Ozone Observation and Modeling Above MLO

[16] Lidar measurements were obtained on the nights of 16, 17, and 18 March 2005. The ozone mixing ratio profiles measured by lidar on 16 March every hour between 0600 UT and 0900 UT are plotted in Figure 3a. Each profile corresponds to a 1-hour integration measurement centered at the time indicated on the figure. On these profiles, the filament is characterized by a layer of enhanced ozone reaching about 1.6 ppmv, as compared to typical climatological values of 1.0 ppmv (as measured, for example, on 9 March and 22 March). In Figure 3a the local ozone peak is reached at 435 K (18.5 km), but this level actually varied from 425 K to 450 K (17 to 20 km) over the few days between the beginning and the end of the event (not shown). Even over the course of one night (Figure 3a), the lidar detected the filament at varying isentropic levels (between 425 K and 435 K).

[17] For this particular case study, MIMOSA-CHIM was initialized on 1 December 2004 and run until 31 March 2005, with regridding and outputs every 6 hours. In order to best match the lidar observation times, an additional run was started on 15 March 2005 at 00 UT, with both regridding and output every 1 hour. All the species in this run were initialized with values obtained from the standard 6-hour MIMOSA-CHIM output on 15 March 2005 at 00 UT. The model ozone profiles above MLO on 16 March between 0600 and 0900 UT are shown in Figure 3b (to be compared with the lidar profiles of Figure 3a). The ozone filament centered near 435 K was actually approaching MLO during the first hours of 16 March, reached MLO at around 0600 UT, and remained above MLO until after 1200 UT. As the filament approaches Hawaii, it can be seen on both the model and lidar profiles as an emerging ozone peak throughout the night.

[18] Figures 4a and 4b show the lidar and modeled profiles respectively, for the following two nights (17 March and 18 March) and for 22 March. Though there is a discrepancy in the actual magnitude of the ozone peak, there is a similar behavior from night to night between observations and model. The peak altitude increases between 16 March and 17 March, does not change on 18 March, then the peak looses its consistency and moves slightly downward on 22 March. The changing peak altitude and magnitude is a consequence of the three-dimensional displacement of the filament with time. The filament can be pictured as a 3-D vortex fold that approached and passed over Hawaii on the night of 16 March. The three-dimensional nature of the filament was confirmed after inspection of many latitude/altitude and time/latitude cross sections of modeled ozone (not shown here). However, the absolute

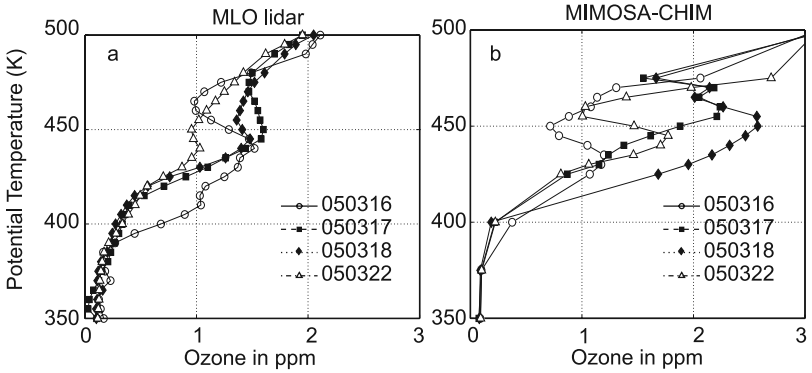

Figure 4. (a) Two-hour integrated ozone profiles measured by the MLO lidar on the nights of 16, 17, 18, and 22 March 2005. (b) MIMOSA-CHIM ozone profiles modeled at 0600 UT on the same nights and location as that measured by lidar.

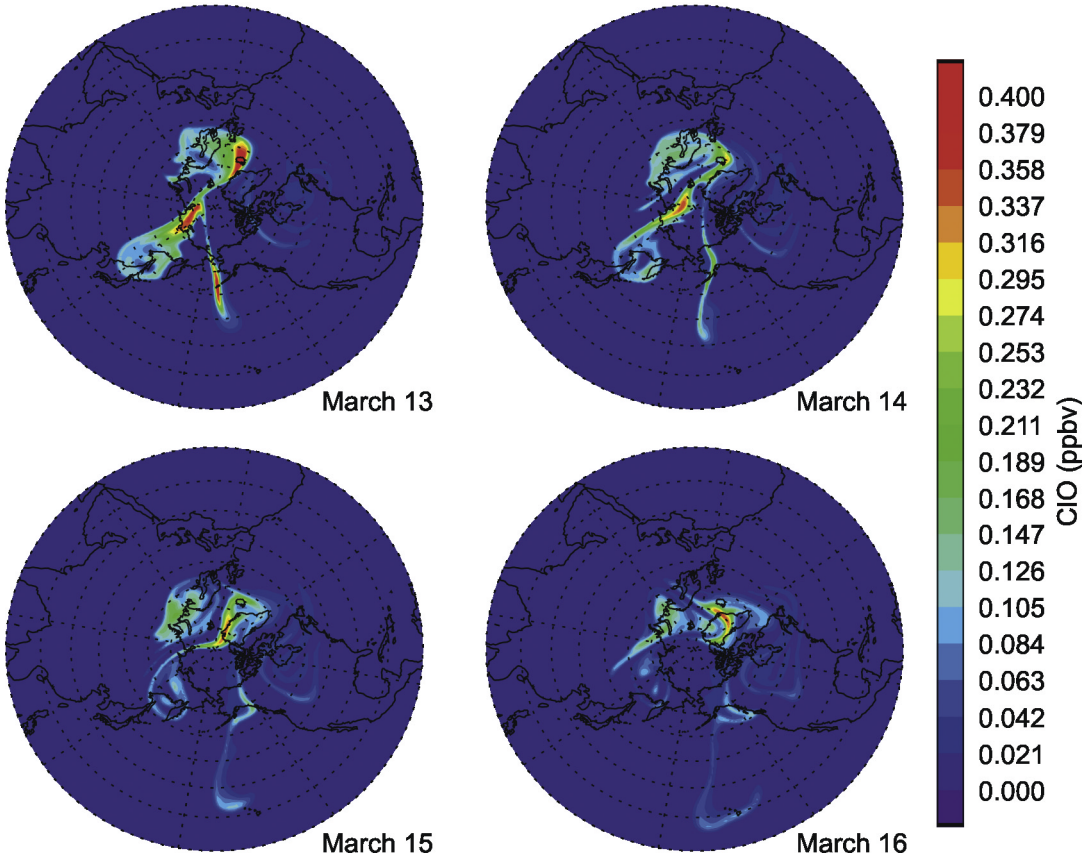

Figure 5. Chlorine monoxide fields at 435 K, calculated by MIMOSA-CHIM between 13 and 16 March at 1800 UT.

position and strength of this peak seems to be slightly off that measured by lidar. In all the observations the peak measured by lidar seems to be at a slightly higher level than that modeled by MIMOSA-CHIM. Considering the main limitations of the model (low vertical resolution at levels above 450 K, and uncertainties in boundary and initial conditions), the observed degree of agreement between lidar and MIMOSA-CHIM remains extremely high.

4. Chemical History of Air Parcel

[19] Figure 5 presents daily global maps of chlorine monoxide (ClO), at 435 K and 1800 UT (day time ClO), between 13 and 16 March from MIMOSA-CHIM. They show the evolution of ClO in the air parcels within the filament during its development and "ejection" out of the vortex. From the maps it is clear that the air mass in the filament that left the polar vortex on 13 March was chemically active containing significant amount of ClO. Also the map on 16 March, when the filament was already in tropical latitudes, shows that the chemically active air mass is transported all the way to the tropics, and chlorine deactivated as the filament passes over MLO.

[20] To complement these maps, a cluster of nine forward and nine backward isentropic trajectories, starting at each grid point within ±1° of longitude and latitude from the location of MLO, and at the mean time of the 16 March lidar measurement, were calculated. The four-times-daily ECMWF isentropic wind fields were used for trajectory calculation. The trajectories were calculated over 15 days in each direction with a time step of 1 hour, and outputs every 6 hours to match the MIMOSA-CHIM output times, allowing the study the chemical history of the air parcels over an entire month. The concentrations of the most important chemical species were extracted from MIMOSA-CHIM, and studied along the calculated trajectories. The diabatic descent of chemical species is taken into account within MIMOSA-CHIM. In the present case study, the isentropic trajectories are a good approximation of the actual three-dimensional trajectories, as the parcels' potential temperature changes do not exceed ±5 K over the course of 15 days. In the worst case scenario, parcels with the largest potential temperature change will be located on isentropic levels immediately above or below that considered at the start of the trajectory. Inspection of the trajectories at multiple levels of 5 K intervals showed that, when considering neighboring levels, there was very little change in the position of the parcels and in the evolution of their composition as modeled by MIMOSA-CHIM. This is confirmed by noting that the thickness of the ozone peak on the profiles in Figures 3a and 3b exceeds 15–20 K.

[21] The top panel of Figure 6 shows the evolution of passive ozone (i.e., advected since 1 December 2004 at the level of reactive ozone at that time) and chemically processed ozone, as modeled by MIMOSA-CHIM along the four trajectories best centered to the "core" of the filament during its MLO overpass. The bottom panel shows the

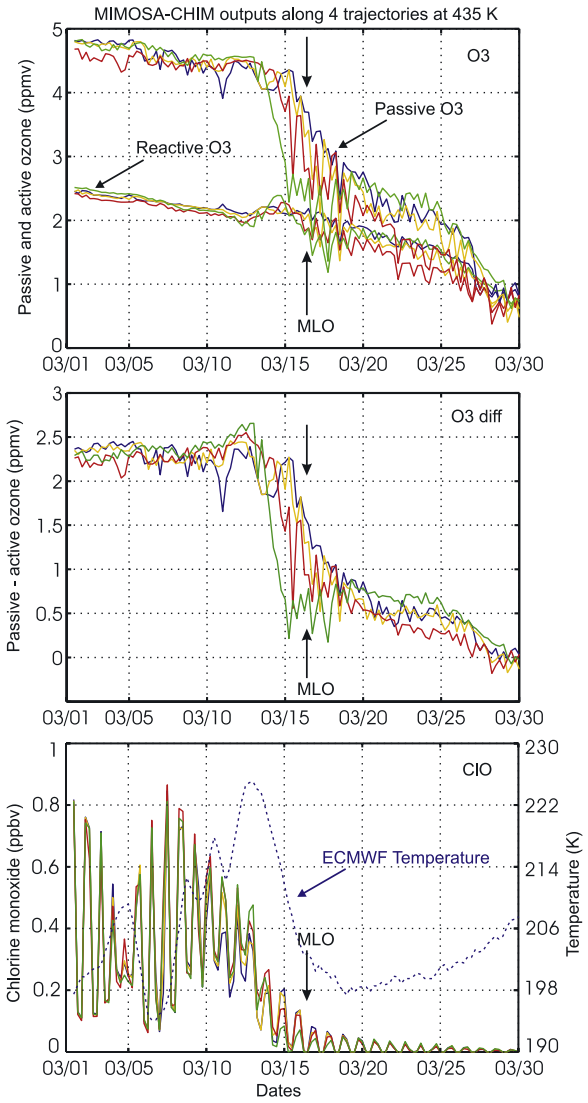

Figure 6. Chemical history of the parcels calculated by MIMOSA-CHIM along four one-month-long isentropic trajectories that passed over MLO on the night of 16 March 2005 (see text for details), including (top) reactive and passive ozone, (middle) difference between passive and reactive ozone, and (bottom) chlorine monoxide and temperature. The date/time at which the parcels passed over MLO is indicated on the plots by arrows.

corresponding evolution of chlorine monoxide (ClO) and temperature modeled along the same four trajectories. The air parcel history can be divided into three periods.

[22] The first period is from 1 to 12–13 March, when the air parcels remain inside the polar vortex. Temperature and ClO are anticorrelated, as we could have expected. On 1 March, when the air parcels were in the polar region, reactive ozone was about 2.5 ppmv and passive ozone about 4.8 ppmv at 435 K. This difference (2.3 ppmv) is due to the chemical ozone depletion involving halogen dominated stratospheric chemistry inside the polar vortex. Ozone loss in other exceptionally cold Arctic winters like 1999/2000 peaks around 440 K and the maximum March ozone loss of about 2 to 2.2 ppmv was reported in various experimental and modeling studies [*Pierce et al.*, 2002; *Eichmann et al.*, 2002; *Grant et al.*, 2003; *Hoppel et al.*, 2002; *Grooß et al.*, 2002; *Schoeberl et al.*, 2002]. MIMOSA-CHIM maximum ozone loss in 1999–2000 at 475 K was about 1.9 ppmv and at 450 K about 2 ppmv at the end of March inside the polar vortex [*Tripathi et al.*, 2006]. The comparison with the above studies of 1999–2000 Arctic winter clearly indicates that the winter 2004/2005 experienced large chlorine activation and exceptionally large ozone loss. Low activated ClO during 4 and 5 March, as seen in the bottom panel of Figure 6, is due to a temporary warming of the air parcels as they traveled through a region of steep horizontal temperature gradient (separating the cold vortex core to the north, and a warmer region to the south). Between 9 and 13 March, there is no heterogeneous production of ClO, and ClO is deactivated for ozone depletion. Until 11 March, the air parcels were well inside the polar vortex, but on 12 March, 1200 UT a significant fraction of the vortex air mass started to separate from the core. Within 24 hours the filament developed as is clearly seen in the 13 March ClO map of Figure 5. The ClO maps indicate that the air mass in the filament on 13 March was chemically well activated (more than 0.3 ppbv of ClO) and was quite separated from the rest of the vortex. During this period reactive ozone along trajectories decreased from 2.5 ppmv to about 2 ppmv.

[23] During the 48 hours from 13 to 15 March, the air parcels along trajectories went through a change in their ozone and ClO content. During that time, they separated from the main polar vortex, and a filament extending south to 35°N latitude formed as shown on the maps of Figure 5. During the parcels' southward travel, the filament remains connected to the main vortex, and reactive ozone after a little increase (from an average 2.1 ppmv to 2.3 ppmv) linearly decreased to about 2 ppmv. The short increase mentioned here will be investigated in the next section. Early in this period, chlorine monoxide concentration drops to 0.45 ppb on 13 March. From 13 to 15 March the ClO

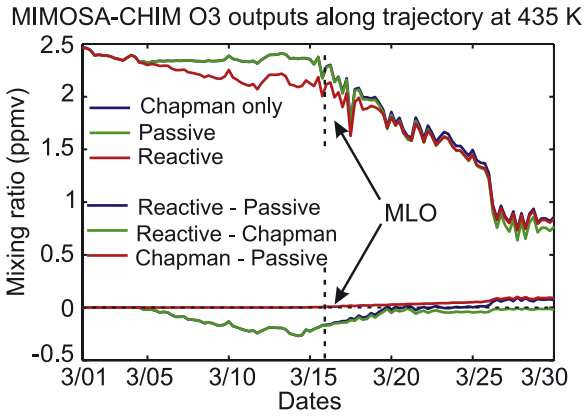

Figure 7. Evolution of ozone as modeled by MIMOSA-CHIM with different assumptions. The red curve shows reactive ozone with the full chemistry included. The green curve shows ozone as if it were a passive tracer. The blue curve shows reactive ozone with Chapman chemistry only. See text for details on the initialization of each test species. The curves close to the zero line show the differences between each species.

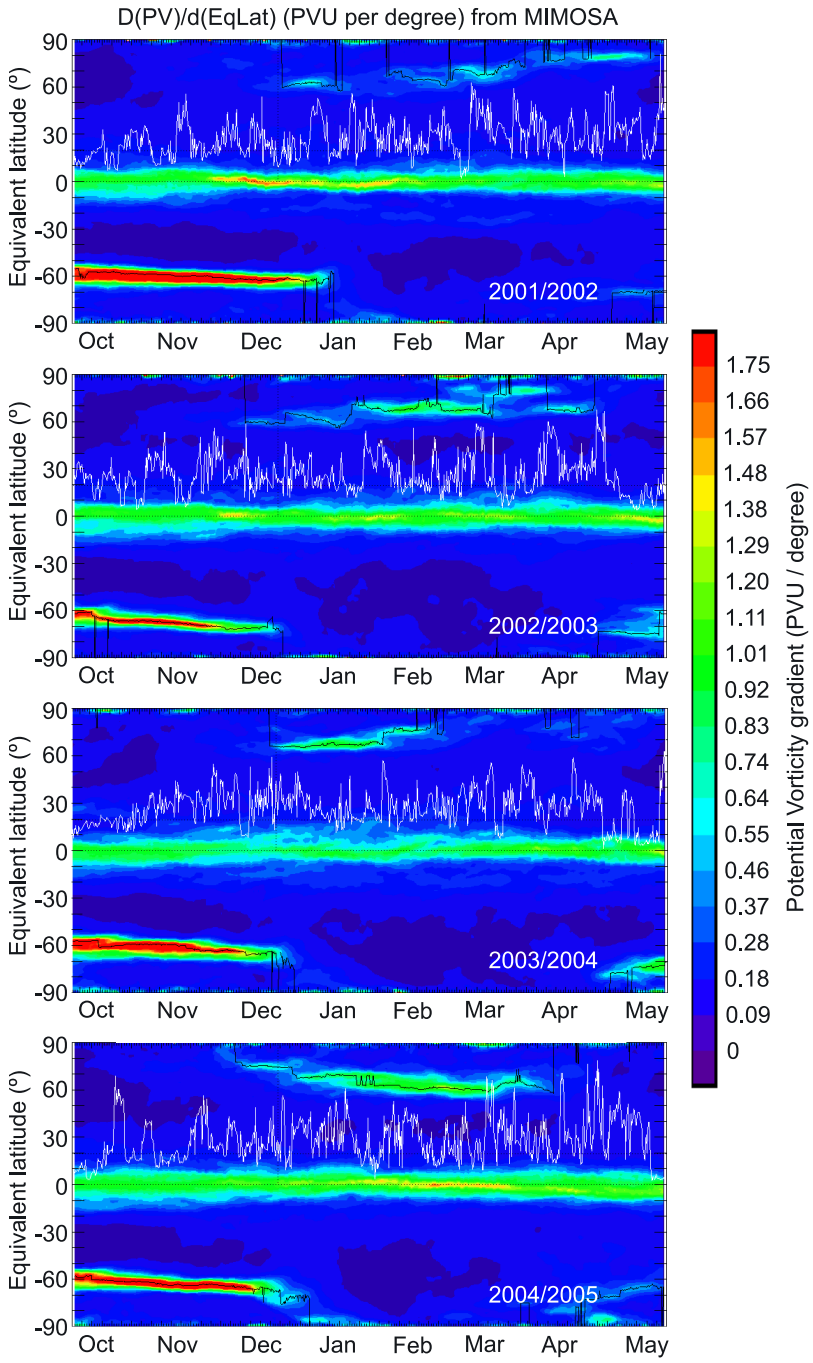

Figure 8. Time series of the meridional gradient of PV with respect to equivalent latitude using the high-resolution advected PV output from MIMOSA during four consecutive winters. Regions of high gradients (green to red) identify transport barriers. The white solid curve superimposed describes the actual equivalent latitude of MLO (one point every 6 hours). The black solid curves describe the northern and southern vortices edge. The crossings of the white curve with the black curve in March 2005 identify the 16 March polar filament event over MLO.

concentration drops to 0.2 ppbv and this chlorine deactivation is inside the filament (Figures 5 and 6). Passive ozone also decreases to about 3.5 to 4 ppmv.

[24] From 15 March on, the difference in concentration between passive and active ozone decreases sharply from about 2.3 ppmv on 14 March to about 0.8 ppmv on 19 March, followed by an approximately linear decrease to almost zero on 29 March. Chlorine monoxide also decreases sharply and is diluted into the surrounding air. This is the third and last part of the parcels' history. The filament is in the midlatitudes and subtropics. Very fast diffusion and mixing along with halogen processing takes place, reducing ClO to less than 0.05 ppbv. Around

29 March, the ozone and passive ozone concentrations reach values typical of the tropical background.

5. Ozone Decrease Within the Filament

[25] To better understand the process of ozone decrease during the filamentation period, two more model test runs were performed. In the first test run, passive ozone (or tracer) concentration values were initialized on 5 March using the concentration values of reactive ozone on that day. The objective of this test was to see the changes (chemical and dynamical) in ozone relative to the 5 March ozone values, all tracer diffusion and transport processes that occurred before this date being ignored. The second test run was to study the relative effect of halogen depletion and natural ozone balance. This time ozone was passed only through the Chapman reactions, all other chemical processing being turned off (referred to as ''Chapman-only'' thereafter). Figure 7 shows the ozone concentration values and their differences in each scenario. Up to 15 March the nearly continuous decrease of fully reactive ozone relative to passive ozone and Chapman-only ozone simply represents halogen ozone depletion in the air mass inside the polar vortex. From 15 March to 19–20 March, the remaining chlorine monoxide is deactivated, and a pure mixing process occurs, leading to the dominant role of the Chapman reactions in the net ozone production.

[26] The strong dilution of tracer calculated by the model along the parcels' trajectories is, to some extent, dependent on the model resolution. This dilution would not be as fast with a higher model resolution such as three points per degree. A sensitivity study would be necessary to clarify this but, as mentioned earlier, the model could not be run at higher resolutions owing to CPU limitations.

6. Concluding Remarks and Perspectives

[27] Three important questions arise from the results of the present case study: (1) How often do filaments of this extent stretch all the way to tropical latitudes? (2) Is there a changing trend in the frequency of such events? (3) What is the net effect of their dispersion in the subtropics as compared to the usual late-spring dilution of the polar vortex?

[28] To help answer question (1), we calculated various northern polar vortex characteristics for the past 6 years. In particular, for each ECMWF global PV field produced since 1999 (6-hour interval, both ECMWF grid and MIMOSA high-resolution grid), we calculated PV as a monotonic function of equivalent latitude following the model of Nash [*Nash et al.*, 1996]. Figure 8 presents two-dimensional time/equivalent latitude maps of identified transport barriers (i.e., meridional gradient of PV with respect to equivalent latitude) obtained from the high-resolution advected PV results of MIMOSA for four consecutive winters since the winter 2001/2002 on the 435 K isentropic surface. The vortex edge corresponds to the region of maximum (red contours) located between 40°N and 85°N, and is identified using black curves superimposed to the color contours. We also overplotted a white curve that depicts the calculated equivalent latitude of Mauna Loa at 435 K (also one point every 6 hours). Interestingly, this curve is not situated at the average latitude of 20°N but instead at the average latitude of 30°N, reflecting a more subtropical than tropical dynamical regime during the boreal winter. More importantly, the regions where the white curve (MLO equivalent latitude) crosses the black curve (northern polar vortex edge) identify occurrences of polar vortex air masses above Mauna Loa (on that isentropic surface). Though air masses from high latitudes (northward of 50°N) occasionally pass over Hawaii (one to three times per winter), the event of 16–19 March 2005 is the only one in the four years shown for which polar vortex air passed over Hawaii. Such an event has not been observed in any of the winters shown here, neither was it during the previous three winters inspected and not shown (1999/2000, 2000/2001, and 2001/2002). This tends to signify that this type of event is very rare and might not have that much of an impact on the tropical or subtropical ozone reservoir. However, we have only inspected surfaces around 435 K, and we have studied the Central Pacific region only. It therefore remains difficult to make any conclusive statement until at least other isentropic surfaces are inspected. In particular, a model study by *Piani et al.* [2002] showed enhanced transport of ozone-depleted air from polar latitudes to the subtropics at isentropic surfaces above 420 K as compared to surfaces below. The authors suggested that this imbalance was due to the upper extension of the subtropical jet acting as a transport barrier. Also, *Orsolini and Grant* [2000] have shown that transport of high-latitude air deep in the subtropics occurred preferably along pathways at the eastern and southern edges of the Aleutian Highs. The filament studied here followed a very similar pathway. Evidence of similar filaments at other longitudes still need to be found. Though *Piani et al.* [2002] have brought one element of answer, questions (2) and (3) remain widely open. Is the present event a consequence of a long-term change in stratospheric circulation and is it likely to reproduce in the future? A worldwide inspection of filaments (other locations and altitudes) seems to be a necessary step forward. Systematic monitoring of this type of event in the future should certainly help provide additional elements of answer.

[29] **Acknowledgments.** The work described in this paper was carried out at the Jet Propulsion Laboratory, California Institute of Technology, under an agreement with the National Aeronautics and Space Administration. The National Research Council (NRC) provided a Resident Research Scholarship to Om Prakash Tripathi during this work. The authors would like to thank Rob Aspey, who assisted in the collection of the lidar data used here. The ECMWF T106 data were made available for NDACC participants at the Norwegian Institute for Air Research (NILU), Norway, and the NCEP operational forecast products were made available by ftp at the National Weather Service–NCEP ftp server: ftpprd.ncep.noaa.gov/pub/data/nccf/com/gfs/prod, USA.

References

Chipperfield, M. P. (1999), Multiannual simulations with a three-dimensional chemical transport model, *J. Geophys. Res.*, *104*(D1), 1781–1806.

Dahlberg, S. P., and K. P. Bowman (1994), Climatology of large-scale isentropic mixing in the Arctic winter stratosphere from analyzed winds, *J. Geophys. Res.*, *99*, 20,585–20,599.

Eichmann, K.-U., M. Weber, K. Bramstedt, and J. P. Burrows (2002), Ozone depletion in Northern Hemisphere winter/spring 1999/2000 as measured by the Global Ozone Monitoring Experiment on ERS-2, *J. Geophys. Res.*, *107*(D20), 8280, doi:10.1029/2001JD001148.

Godin, S., M. Marchand, A. Hauchecorne, and F. Lefèvre (2002), Influence of Arctic polar ozone depletion on lower stratospheric ozone amounts at Haute-Provence Observatory (43.92°N, 5. 71°E), *J. Geophys. Res.*, *107*(D20), 8272, doi:10.1029/2001JD000516.

Grant, W. B., E. V. Browell, C. F. Butler, S. C. Gibson, S. A. Kooi, and P. von der Gathen (2003), Estimation of Arctic polar vortex ozone loss during the winter of 1999–2000 using vortex-averaged airborne differential absorption lidar ozone measurements referenced to N2O isopleths, *J. Geophys. Res.*, *108*(D10), 4309, doi:10.1029/2002JD002668.

Grooß, J.-U., et al. (2002), Simulation of ozone depletion in spring 2000 with the Chemical Lagrangian Model of the Stratosphere (CLaMS), *J. Geophys. Res.*, *107*(D20), 8295, doi:10.1029/2001JD000456.

Hanson, D., and K. Mauersberger (1988), Laboratory studies of the nitric acid trihydrate: Implications for the south polar stratosphere, *Geophys. Res. Lett.*, *15*, 855–858.

Hauchecorne, A., S. Godin, M. Marchand, B. Heese, and C. Souprayen (2002), Quantification of the transport of chemical constituents from the polar vortex to midlatitudes in the lower stratosphere using the high-resolution advection model MIMOSA and effective diffusivity, *J. Geophys. Res.*, *107*(D20), 8289, doi:10.1029/2001JD000491.

Hoppel, K., R. Bevilacqua, G. Nedoluha, C. Deniel, F. Lefèvre, J. Lumpe, M. Fromm, C. Randall, J. Rosenfield, and M. Rex (2002), POAM III observations of arctic ozone loss for the 1999/2000 winter, *J. Geophys. Res.*, *107*(D20), 8262, doi:10.1029/2001JD000476.

Knudsen, B. M., and J. U. Grooß (2000), Northern midlatitude stratospheric ozone dilution in spring modeled with simulated mixing, *J. Geophys. Res.*, *105*(D5), 6885–6890.

Leblanc, T., and I. S. McDermid (2000), Stratospheric ozone climatology from lidar measurements at Table Mountain (34.4°N, 117.7°W) and Mauna Loa (19.5°N, 155.6°W), *J. Geophys. Res.*, *105*, 14,613–14,623.

Leblanc, T., and I. S. McDermid (2001), Quasi-biennial oscillation signatures in ozone and temperature observed by lidar at Mauna Loa, Hawaii (19.5°N, 155.6°W), *J. Geophys. Res.*, *106*, 14,869–14,874.

Leblanc, T., I. S. McDermid, and A. Hauchecorne (2004), A study of ozone variability and its connection with meridional transport in the northern Pacific lower stratosphere during summer 2002, *J. Geophys. Res.*, *109*, D11105, doi:10.1029/2003JD004027.

Leblanc, T., O. P. Tripathi, I. S. McDermid, L. Froidevaux, N. J. Livesey, W. G. Read, and J. W. Waters (2006), Simultaneous lidar and EOS MLS measurements, and modeling, of a rare polar ozone filament event over Mauna Loa Observatory, Hawaii, *Geophys. Res. Lett.*, *33*, L16801, doi:10.1029/2006GL026257.

Lefèvre, F., G. P. Brasseur, I. Folkins, A. K. Smith, and P. Simon (1994), Chemistry of the 1991/1992 stratospheric winter: Three dimensional model simulation, *J. Geophys. Res.*, *99*, 8183–8195.

Lefèvre, F., F. Figarol, K. S. Carslaw, and T. Peter (1998), The 1997 Arctic ozone depletion quantified from three-dimensional model simulations, *Geophys. Res. Lett.*, *25*, 2425–2428.

Marchand, M., S. Godin, A. Hauchecorne, F. Lefèvre, S. Bekki, and M. Chipperfield (2003), Influence of polar ozone loss on northern mid-latitudes regions estimated by a high-resolution chemistry transport model during winter 1999–2000, *J. Geophys. Res.*, *108*(D5), 8326, doi:10.1029/2001JD000906.

Mariotti, A., M. Moustaoui, B. Legras, and H. Teitelbaum (1997), Comparison between vertical ozone, soundings, reconstructed potential vorticity maps by contour advection with surgery, *J. Geophys. Res.*, *102*, 6131–6142.

McDermid, I. S., S. M. Godin, and L. O. Lindqvist (1990), Ground-based laser DIAL system for long-term measurements of stratospheric ozone, *Appl. Opt.*, *29*, 3603–3612.

McDermid, I. S., T. D. Walsh, A. Deslis, and M. L. White (1995), Optical-systems design for a stratospheric lidar system, *Appl. Opt.*, *34*, 6201–6210.

Murray, F. W. (1967), On the computation of saturation vapour pressure, *J. Appl. Meteorol.*, *6*, 203–204.

Nash, E. R., P. A. Newman, J. E. Rosenfield, and M. E. Schoeberl (1996), An objective determination of the polar vortex using Ertel's potential vorticity, *J. Geophys. Res.*, *101*, 9471–9478.

Norton, W. A., and M. P. Chipperfield (1995), Quantification of the transport of chemically activated air from the Northern Hemisphere polar vortex, *J. Geophys. Res.*, *100*, 25,817–25,840.

Orsolini, Y. J., and W. B. Grant (2000), Seasonal formation of nitrous oxide laminae in the low and mid latitude stratosphere, *Geophys. Res. Lett.*, *27*, 1119–1122.

Orsolini, Y. J., G. Hansen, U.-P. Hoppe, G. L. Manney, and K. H. Fricke (1997), Dynamical modelling of wintertime lidar observations in the Arctic: Ozone laminae and ozone depletion, *Q. J. R. Meteorol. Soc.*, *123*, 785–800.

Piani, C., W. A. Norton, A. M. Iwi, E. A. Ray, and J. W. Elkins (2002), Transport of ozone-depleted air on the breakup of the stratospheric polar vortex in spring/summer 2000, *J. Geophys. Res.*, *107*(D20), 8270, doi:10.1029/2001JD000488.

Pierce, R. B., et al. (2002), Large-scale chemical evolution of the Arctic vortex during the 1999/2000 winter: HALOE/POAM III Lagrangian photochemical modeling for the SAGE III—Ozone Loss and Validation Experiment (SOLVE) campaign, *J. Geophys. Res.*, *107*(D5), 8317, doi:10.1029/2001JD001063.

Plumb, R. A., D. W. Waugh, R. J. Atkinson, P. A. Newman, L. R. Lait, M. R. Schoeberl, E. V. Browell, A. J. Simmons, and M. Loewenstein (1994), Intrusion into the lower stratospheric Arctic vortex during the winter of 1991/1992, *J. Geophys. Res.*, *99*, 1089–1105.

Pruppacher, H. R., and J. D. Klett (1997), *Microphysics of Clouds and Precipitation*, Springer, New York.

Rabier, F., H. Jarvinen, E. Klinker, J.-F. Mahfouf, and A. Simmons (2000), The ECMWF operational implementation of four-dimensional variational assimilation, I, Experimental results with simplified physics, *Q. J. R. Meteorol. Soc.*, *126*, 1143–1170.

Reid, S. J., et al. (1998), A study of ozone laminae using diabatic trajectories, contour advection and photochemical trajectory model simulations, *J. Atmos. Chem.*, *30*, 187–207.

Sander, S. P., et al. (2003), Chemical kinetics and photochemical data for use in atmospheric studies, *Eval. 15*, *JPL Publ. 02-25*.

Schoeberl, M. R., et al. (2002), An assessment of the ozone loss during the 1999–2000 SOLVE/THESEO 2000 Arctic campaign, *J. Geophys. Res.*, *107*(D20), 8261, doi:10.1029/2001JD000412.

Shine, K. P. (1987), The middle atmosphere in the absence of dynamical heat fluxes, *Q. J. R. Meteorol. Soc.*, *113*, 603–633.

Stolarski, R. S., R. Bajkov, L. Bishop, C. Zerefos, J. Staehelin, and J. Zawodny (1992), Measured trend in stratospheric ozone, *Science*, *256*, 342–349.

Tripathi, O. P., et al. (2006), High resolution simulation of recent Arctic and Antarctic stratospheric chemical ozone loss compared to observations, *J. Atmos. Chem.*, in press.

Tuck, A. F., et al. (1992), Polar stratospheric cloud processed air and potential vorticity in the Northern Hemisphere lower stratosphere at mid-latitudes during winter, *J. Geophys. Res.*, *97*, 7883–7904.

Waibel, A. E., et al. (1999), Arctic ozone loss due to denitrification, *Science*, *283*, 2064–2069.

Waugh, D. W., et al. (1994), Transport out of the lower stratosphere Arctic vortex by Rossby wave breaking, *J. Geophys. Res.*, *99*, 1071–1088.

World Meteorological Organization (WMO) (1998), Assessment of trends in the vertical distribution of ozone, *Rep. 43*, Geneva.

A. Hauchecorne, F. Lefèvre, and M. Marchand, Service d'Aeronomie du CNRS, Université Pierre et Marie Curie, 4 Place Jussieu, F-75252 Paris Cedex 05, France.

T. Leblanc, I. S. McDermid, and O. P. Tripathi, Table Mountain Facility, Jet Propulsion Laboratory, California Institute of Technology, Wrightwood, CA 92397-0367, USA. (leblanc@tmf.jpl.nasa.gov)